Supplementary Information:

Molecular oxygen activation by atomic Fe-moieties on MnO_2 for enhanced remediation of parachlormetaxylenol wastewater

Huiji Xiao[1], Wenli Zhang[1], Chenxi Zhu[1], Kewei Lv[2], Yun Wang[1], Bing Xie[3], Xiaoming Zou[1], Xubiao Luo[1], Yanbo Zhou ✉ [1,2,4]

1-School of Life Sciences, Key Laboratory of Jiangxi Province for Functional Biology and Pollution Control in Red Soil Regions, Jinggangshan University, Ji'an, 343009, China

2-State Key Laboratory of Coal Liquification, Gasification and Utilization with High Efficiency and Low Carbon Technology, East China University of Science and Technology, Shanghai, 200237, China

3-Shanghai Engineering Research Center of Biotransformation of Organic Solid Waste, School of Ecological and Environmental Sciences, East China Normal University, Shanghai 200241, China

4-Key Laboratory of Environmental Risk Assessment and Control on Chemical Process, Ministry of Ecology and Environment, East China University of Science and Technology, Shanghai, 200237, China

Totally 43 pages including 8 Texts, 7 Tables, and 23 Figures.

Text S1. Reagents and Materials

Potassium persulfate monohydrate ($K_2S_2O_8 \cdot H_2O$), Manganese(II) chloride tetrahydrate ($MnCl_2 \cdot 4H_2O$), Iron(III) nitrate nonahydrate ($Fe(NO_3)_3 \cdot 9H_2O$), potassium iodide (KI), Ammonium oxalate ($(NH_4)_2C_2O_4 \cdot H_2O$), Potassium permanganate ($KMnO_4$), Parachlorometaxylenol (PCMX, C_8H_9ClO), Hydrochloric acid (HCl), Sodium hydroxide (NaOH), Furfuryl alcohol (FFA, $C_5H_6O_2$), Sodium dihydrogen phosphate (NaH_2PO_4), Sodium carbonate (Na_2CO_3), Sodium nitrate ($NaNO_3$), Sodium bicarbonate ($NaHCO_3$), Terephthalic acid ($C_8H_6O_4$) were provided by Aladdin Reagents Co., Ltd.. Ethanol (EtOH, C_2H_5OH), Benzoquinone ($C_6H_4O_2$), Concentrated sulfuric acid (H_2SO_4), Sodium chloride (NaCl), Sodium persulfate ($Na_2S_2O_8$), Sodium sulfate (Na_2SO_4), Sulfamethazine ($C_{12}H_{14}N_4O_2S$), Sulfadiazine ($C_{10}H_{10}N_4O_2S$) were provided by Sinopharm Chemical Reagent Co. Ltd., China. Chloroform ($CHCl_3$), Para-chloro-meta-xylenol (C_7H_7ClO), Humic acid (HA), Methanol (MeOH, CH_3OH), tert-Butanol (TBA, $C_4H_{10}O$), 5,5-dimethyl-1-pyrrolidine-N-oxide (DMPO), 4-amino-2,2,6,6-tetramethylpiperidine (TEMP), and β-carotene ($C_{40}H_{56}$) were purchased from Sigma Chemical Co. All working solutions were prepared in deionized water (18.2 MΩ·cm resistivity, Millipore Milli-Q system).

Text S2. Preparation Methods of Catalyst

2.1 Preparation of $Fe_{0.1}$-Mn-350: $Fe_{0.1}$-Mn-350 was prepared via a hydrothermal-calcination method. 1.58 g of potassium permanganate ($KMnO_4$) was dissolved in 30 mL of deionized water, and then 20 mL of a 35.5 g/L ammonium oxalate solution was added dropwise to the $KMnO_4$ solution. After stirring for 0.5 hours, the ferric nitrate solution was transferred into the above mixture and stirred again at room temperature for 1 hour. The mixture was then transferred into an autoclave and placed in an oven at 180 °C for a hydrothermal reaction for 24 hours. After cooling to room temperature, the product was washed alternately with ethanol and deionized water three times and dried in vacuum at 105 °C for 12 hours. The resulting dark gray powder was placed in an alumina crucible and calcined for 2 hours in air at a set temperature. By varying the mass of ferric nitrate, catalysts with different iron contents were obtained. The catalysts were denoted as Fe_x-Mn, where x represents the ratio of Fe to Mn (n(Fe)/n(Mn)=x%). The catalysts obtained at different calcination temperatures were denoted as Fe_x-Mn-N (N=250, 350, 450, indicating calcination temperatures of 250 °C, 350 °C, and 450 °C, respectively). The synthesis process of the materials is shown in **Fig. S1**.

2.2 Preparation of MnO_2: MnO_2 was prepared in the same manner as Fe_x-Mn-N, except that no ferric nitrate was added.

Text S3. Analytical Methods

Catalyst Crystal Structure Analysis. A suitable amount of catalyst powder is dispersed on a silicon wafer, and the crystal structure and degree of crystallinity of the material are tested using an X-ray diffractometer (XRD). The test employs a Rigaku D/max2550VB/PC X-ray diffractometer (manufactured by Rigaku Corporation, Japan), with a measurement rate of 5° per minute over an angular range of 10° to 80°.

Morphological Structure Analysis. The morphology and microstructure of the iron-manganese bimetallic material are characterized using a GeminiSEM 500 field-emission scanning electron microscope with a magnification range of 500 to 300,000 times, and a JEM-1400 transmission electron microscope with a magnification range of 50 to 800,000 times. For TEM testing, the iron-manganese bimetallic material is dispersed in anhydrous ethanol solution and sonicated for several minutes to prevent aggregation that could affect observation. A small amount of the dispersed solution is then dropped onto a microgrid copper mesh, allowed to dry, and then sent for testing.

Element Valence State Analysis. A Thermo Scientific X-ray photoelectron spectrometer is used to analyze the valence states of elements such as O, Fe, and Mn in the iron-manganese bimetallic material, and to compare the differences in elemental composition on the surface of the material before and after cyclic reactions. In XPS testing, X-rays are irradiated onto the material surface, and due to the different binding energies and elemental types within the material, the kinetic energy and quantity of inner electrons ionized into free electrons also vary, thus obtaining information on the elemental composition and valence states of the material.

Metal Element Content Analysis in Solution. An inductively coupled plasma optical emission spectrometer (ICP-OES, Agilent, 167nm-785nm/725) is used to determine the content of metals such as iron and manganese in the iron-manganese bimetallic catalyst, and to detect the concentration of iron and manganese ions leached during the reaction. In the test, an appropriate amount of catalyst is placed in a digestion tube, 10 mL of aqua regia is added to completely dissolve the catalyst, and the

ICP-OES is used for measurement. After the measurement, quantitative analysis is performed based on the obtained data. To reduce testing errors, each set of materials is tested three times, and the average value is taken as the result.

Electrochemical Analysis. Electrochemical analysis is an important method in materials science research. In the test, a composite material coated with catalyst is used as the working electrode, platinum is chosen as the counter electrode, and a saturated mercury-ammonia electrode is used as the reference electrode. Within a three-electrode system, electrochemical analysis instruments are combined to sequentially use electrochemical impedance spectroscopy (EIS), cyclic voltammetry (CV), and linear sweep voltammetry (LSV) for electrochemical property evaluation, thereby studying the electron transfer process within the system.

Text S4. Organic Pollutant Determination

The concentrations of organic pollutants were quantified with HPLC (HITACHI Primaide 1410 UV Detector), where the compounds were separated with an Innoval ODS-2 C18 column (4.6 × 150 mm, 5 μm) in an isocratic mode of elution at 26 °C coupled with a UV-visible detector working at 200~300 nm. A solution of water and acetonitrile (50%/50%$_{vol/vol}$ (water/ acetonitrile)) was eluted at 1 mL/min as the mobile phase (Table S1). Calibration curves were obtained by using the pure standards of BPA, PCMX, phenol, SA, SDZ (purity > 99%, Sigma).

The kinetics (k_{obs}) of the pollutants catalysis degradation data was fitted by first-order equation which given as Eq. S1:

$$ln(C_t/C_0) = -k_{obs} \times t \qquad \text{(S1)}$$

Where C_t was the concentration of pollutants at t time (mg/L), C_0 was the original concentration of contaminants (mg/L), k_{obs} was the degradation rate constant (min^{-1}).

Liquid chromatography-mass spectrometry (LC-MS) was employed to analyze the intermediate degradation products of para-chlorometaxylenol (PCMX) and bisphenol A (BPA) in the advanced oxidation system catalyzed by iron-manganese bimetallic catalysts. To activate the solid-phase extraction (SPE) column, 10 mL of methanol, 10 mL of a methanol-water mixture in equal volumes, and 10 mL of ultrapure water were sequentially passed through a C18 SPE column. The catalytic reaction was initiated, and when the reaction reached the intermediate stage, the reaction mixture was quickly poured into a filtration apparatus to separate the solid catalyst from the reaction solution. The collected filtrate was slowly passed through the extraction column, allowing the intermediate degradation products to be enriched within the column. Methanol (5-8 mL) was used to elute the enriched intermediate degradation products from the column into a vial, and nitrogen gas was

employed to accelerate the evaporation of methanol, concentrating the sample to less than 1 mL, which was then submitted for analysis.

Text S5. Analysis of Reactive Species

5.1 Electron paramagnetic resonance (EPR) tests: EPR spectra were collected with an A100, Bruker ESR spectrometer. DMPO (5,5-dimethyl-1-pyrrolidine-N-oxide) and TEMP (4-amino-2,2,6,6-tetramethylpiperidine) were used as the spin-trapping agents in the ESR experiments. DMPO were used as a spin trap to detect $^{\bullet}OH$, and $O_2^{\bullet-}$. TEMP/water solution was employed as a spin trap for singlet oxygen ($^1O_2$). For the EPR measurements of $^{\bullet}OH$, and $O_2^{\bullet-}$, 1 mL of the sample after 1 min of electrolysis was immediately mixed with 10 μL of the trap agent [1] and then the mixture was immediately loaded into a capillary tube for testing. To monitor the generation of $O_2^{\bullet-}$ by EPR, it should be noted that high-concentration methanol solution (the volume ratio of methanol to water was set as 1:1) was utilized as the electrolyte.

5.2 $^{\bullet}OH$ determination: The reaction of $^{\bullet}OH$ with phthalic acid produces a fluorescent signal. Therefore, phthalic acid is used to detect the generation of $^{\bullet}OH$ in a system. In the experiment, 50 mL of a 10 mM phthalic acid solution was taken, and a catalyst was added to initiate the reaction. At specific time intervals, 1 mL of the sample was taken and filtered, then diluted to 3 mL with deionized water for subsequent fluorescence detection.

5.3 $^1O_2$ determination: The absorption spectrum of 9,10-anthraquinonyl-bis(methylene)dimalonic acid (ABDA) has a characteristic band around 378 nm. This compound can specifically capture singlet oxygen ($^1O_2$) by forming an endoperoxide product, which leads to the disappearance of its characteristic absorption band. In the experiment, 50 mL of a 10 mM ABDA solution was prepared, and a catalyst was added to initiate the reaction. Samples were taken at specific time points, filtered, and the fluorescence intensity at 378 nm was detected and recorded.

Text S6. Biotoxicity Analysis by T.E.S.T.

Based on the LC-MS analysis, the mass-to-charge ratios (m/z) of the intermediate products and the structural formulas of the degradation products can be determined. Furthermore, the possible degradation pathways of pollutants in the system can be inferred. The Toxicity Estimation Software Tool (T.E.S.T.) is employed to assess the developmental toxicity and acute toxicity information of the degradation intermediates of PCMX.

Mass-to-Charge Ratios (m/z) and Structural Formulas: LC-MS analysis provides the m/z values of the intermediate products, which are crucial for identifying the molecular and structural information of the degradation products. The specific m/z values and structural formulas would be detailed in the LC-MS output, which can be used to elucidate the degradation pathways of the pollutants.

Degradation Pathways: By analyzing the m/z values and structural formulas of the intermediates, one can deduce the potential degradation pathways of the pollutants within the system. This involves understanding how the initial pollutants transform into intermediates and eventually into less harmful or non-harmful products.

Toxicity Estimation Using T.E.S.T.: The Toxicity Estimation Software Tool (T.E.S.T.) is utilized to predict the toxicity of the degradation intermediates of PCMX. T.E.S.T. employs various Quantitative Structure-Activity Relationship (QSAR) methodologies to estimate toxicity from molecular structure, allowing users to assess the developmental and acute toxicity of the intermediates.

Text S7. Zebrafish Toxicity Tests

The different treatment groups (the control sample, original PCMX-containing water sample, PCMX treated by $Fe_{0.1}$-Mn-350/O_2 and MnO_2/O_2 systems, respectively) were serially diluted at equal ratios and stored at -4 ˚C for subsequent use. One healthy sexually mature female and one male zebrafish were selected from the aquarium and placed in a mating tank. The following morning, fertilized eggs were transferred to Petri dishes containing embryo medium (5 mM NaCl, 0.17 mM KCl, 0.33 mM $CaCl_2$, 0.33 mM $MgSO_4$). At 8 hours post-fertilization (hpf), normally developing zebrafish embryos were randomly selected and distributed into 6-well plates (20 embryos per well). After exposure to various treatment groups until 72 hpf, zebrafish embryo mortality and spontaneous hatching rates were recorded. Larvae were then anesthetized with 200 mg L^{-1} tricaine and immobilized using 1% methylcellulose [2]. Images were acquired using a stereomicroscope (M205 F, Leica, Germany), and larval malformation rates were quantified.

Text S8. DFT calculation

To investigate the adsorption and electronic transfer processes of oxygen on the $Fe_{0.1}$-Mn-350 catalyst surface, the initial step involves constructing the catalyst surface model. Typically, low-index crystallographic planes such as (111) and (100) are selected due to their prevalence and representativeness in practical catalysts [3, 4], with surface defects like oxygen vacancies also incorporated into the model if present. Oxygen molecules (O_2) or atoms (O) are subsequently introduced as adsorbates to simulate the adsorption process. For the adsorption process calculations, the adsorption energy (E_{ads}) of oxygen is determined using the formula $E_{ads}=E_{total}-(E_{surface}+E_{oxygen})$, where E_{total}, $E_{surface}$, and E_{oxygen} represent the total energy of the adsorption system, the energy of the catalyst surface, and the energy of the oxygen molecule or atom, respectively. The magnitude of the adsorption energy reflects the catalyst's affinity for oxygen, with more negative values indicating stronger adsorption capabilities.

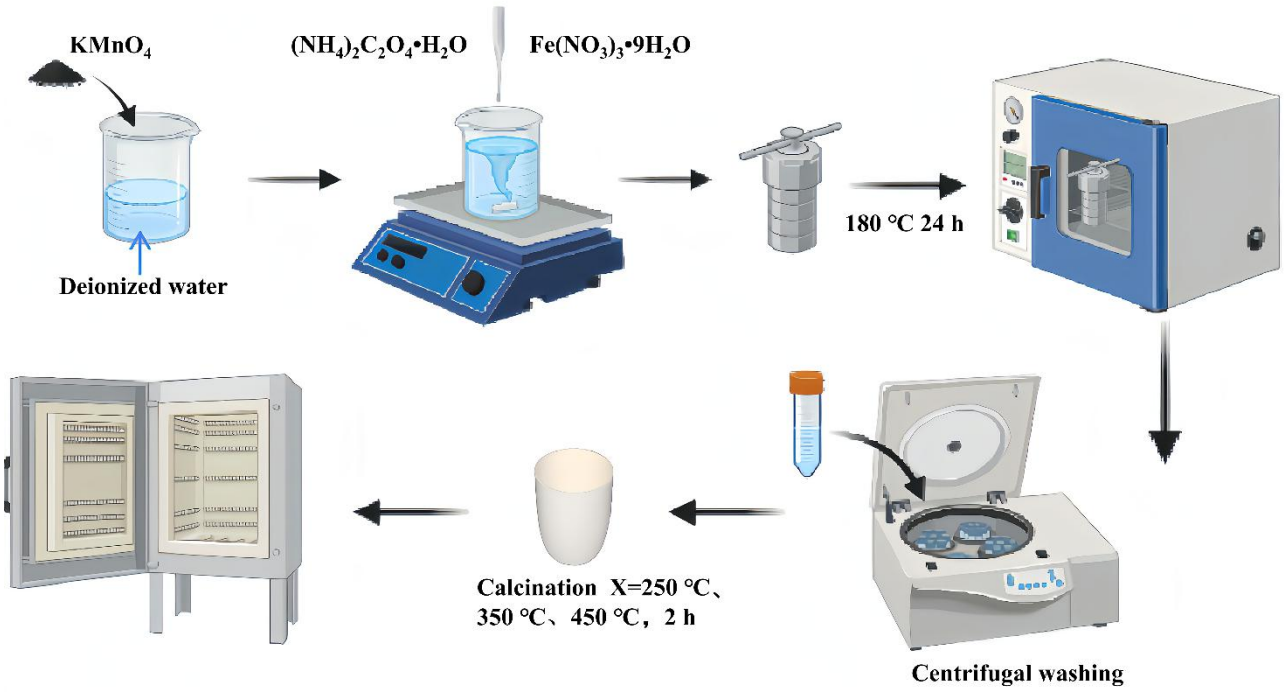

Figure S1. Schematic of the fabrication of $Fe_{0.1}$-Mn-350.

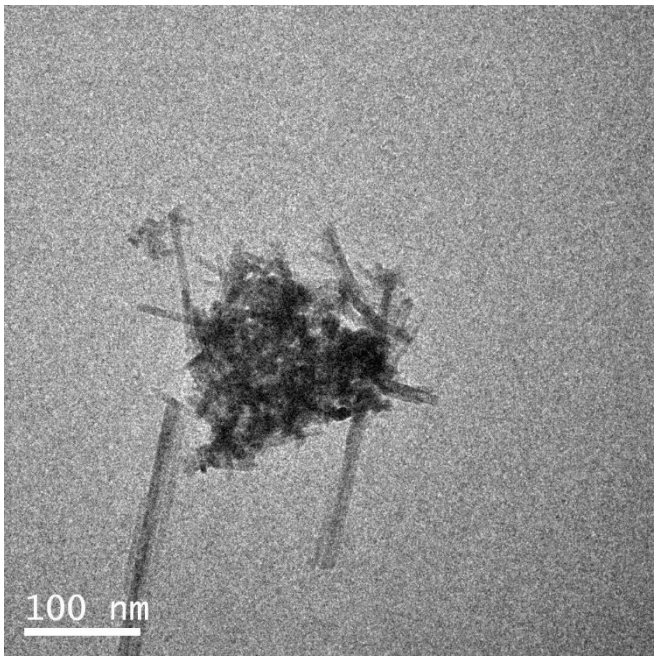

Figure S2. TEM images of MnO_2.

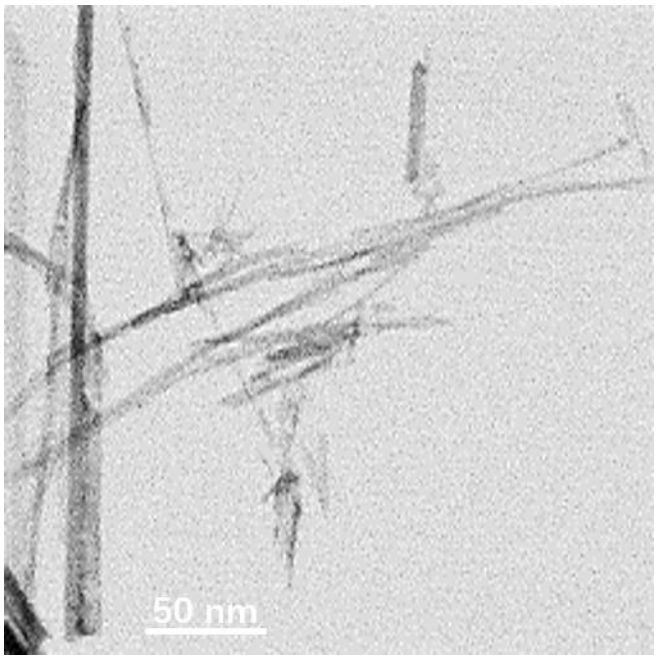

Figure S3. TEM images of $Fe_{0.1}$-Mn-350.

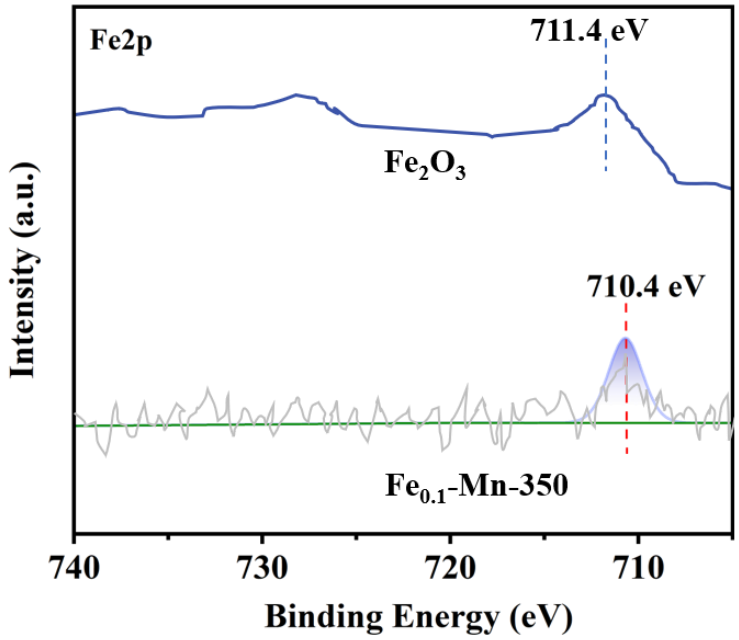

Figure S4. XPS spectra of Fe 2p in Fe_2O_3 and $Fe_{0.1}$-Mn-350.

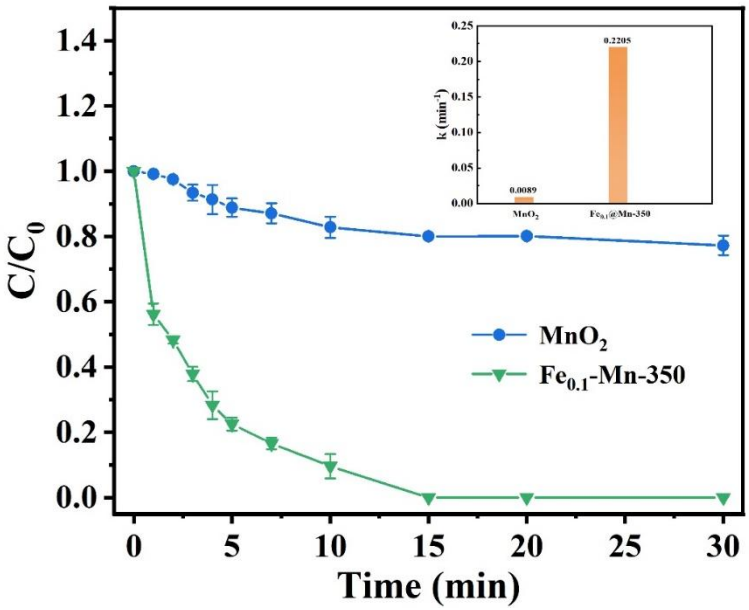

Figure S5. Degradation efficiencies and kinetics of PCMX by MnO_2 and Fe-modified MnO_2 catalysts. Conditions: $[PCMX]_0 = 20$ mg/L, [Cat.] = 0.2 g/L, $pH_0 = 5.6$.

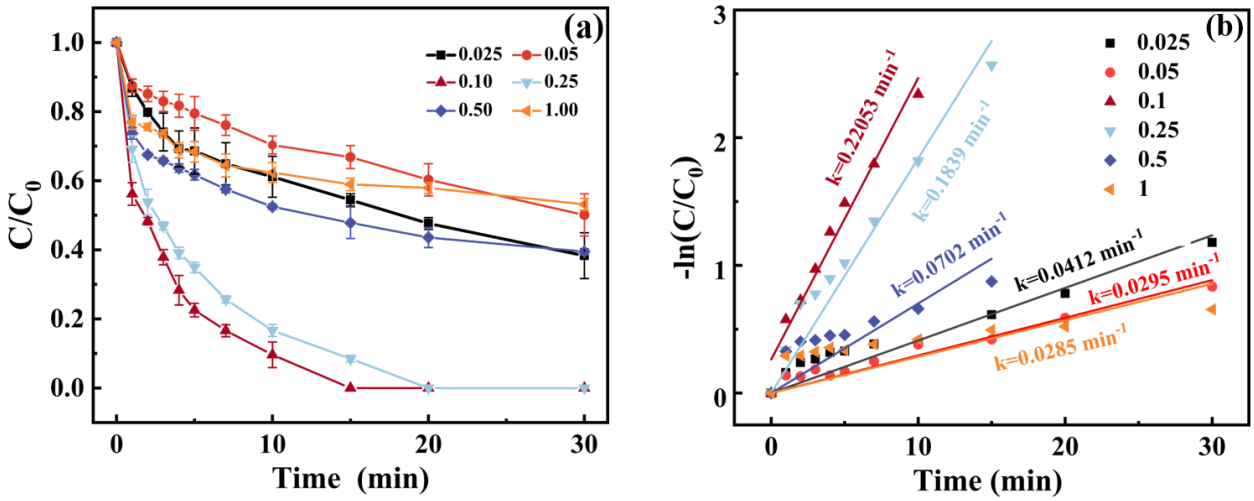

Figure S6. Degradation efficiency (a) and kinetics (b) of PCMX by Fe_x-Mn-350 with different iron-manganese ratios. Conditions: $[PCMX]_0$ = 20 mg/L, [Cat.] = 0.2 g/L, pH_0 = 5.6, n(Fe)/n(Mn)=0.025~1%.

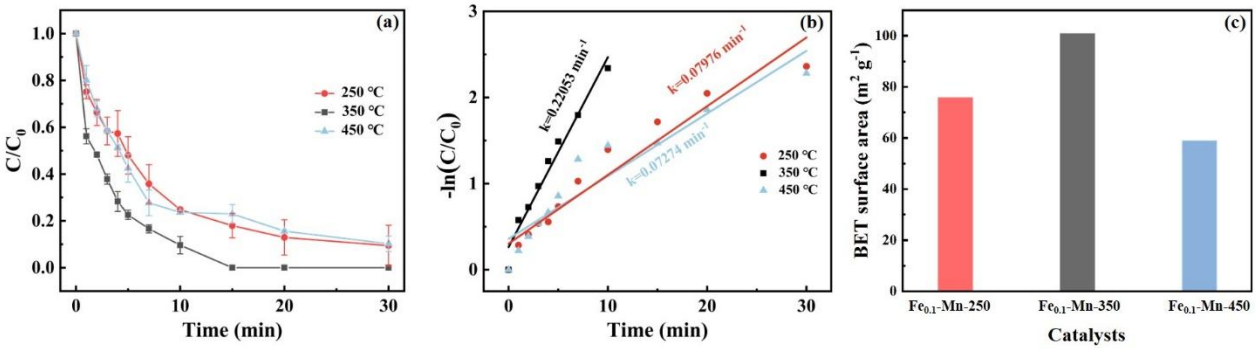

Figure S7. Degradation efficiency (a) and kinetics (b) of PCMX by $Fe_{0.1}$-Mn-N at different calcination temperatures; BET surface area of $Fe_{0.1}$-Mn-N (c). Conditions: $[PCMX]_0$ = 20 mg/L, [Cat.] = 0.2 g/L pH_0 = 5.6.

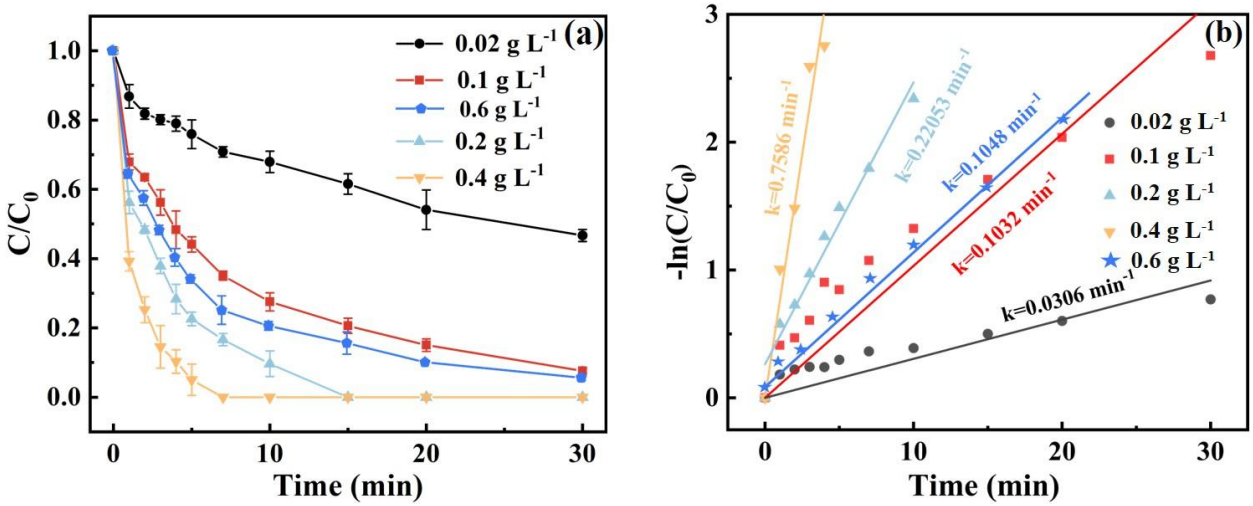

Figure S8. Degradation efficiency (a) and kinetics (b) of PCMX by $Fe_{0.1}$-Mn-350/O_2 system at different catalyst dosages. Conditions: $[PCMX]_0$ = 20 mg/L, pH_0 = 5.6.

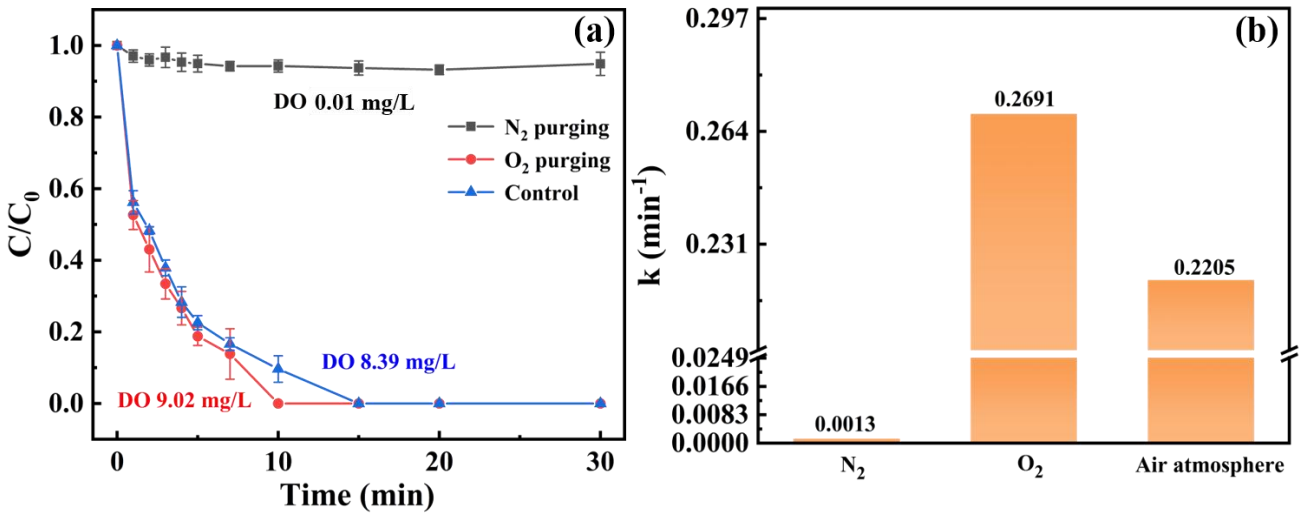

Figure S9. Degradation efficiency (a) and kinetics (b) of PCMX by $Fe_{0.1}$-Mn-350 under different atmospheres. Conditions: $[PCMX]_0$ = 20 mg/L, [Cat.] = 0.2 g/L, pH_0 = 5.6.

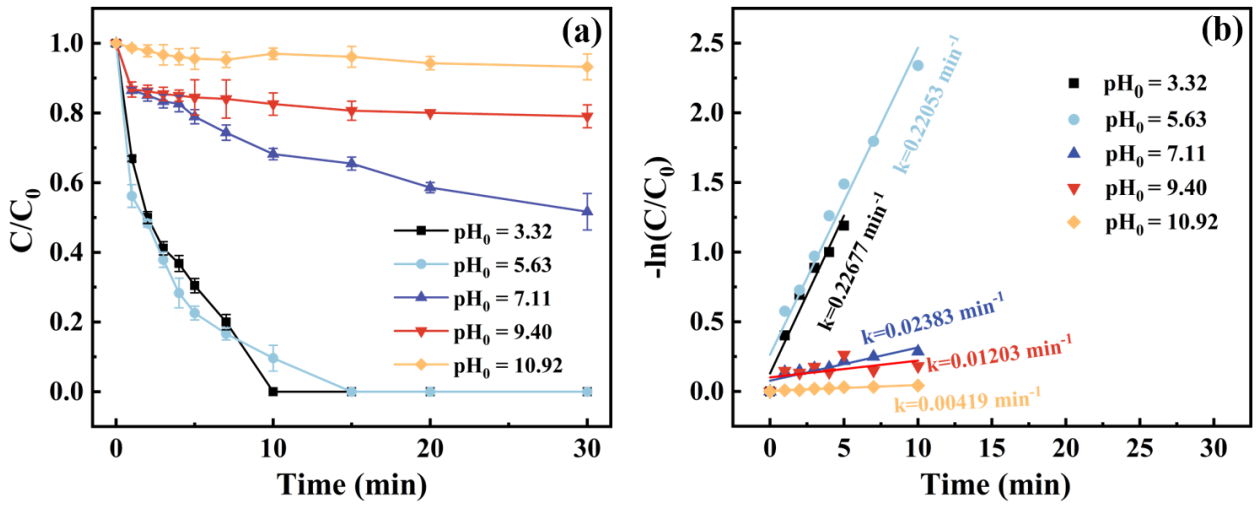

Figure S10. Effect of initial pH on the degradation efficiency (a) and kinetics (b) of PCMX in $Fe_{0.1}$-Mn-350/O_2 system. Conditions: $[PCMX]_0$=20 mg/L, [Cat.] = 0.02~0.4 g/L, pH_0 = 3~11.

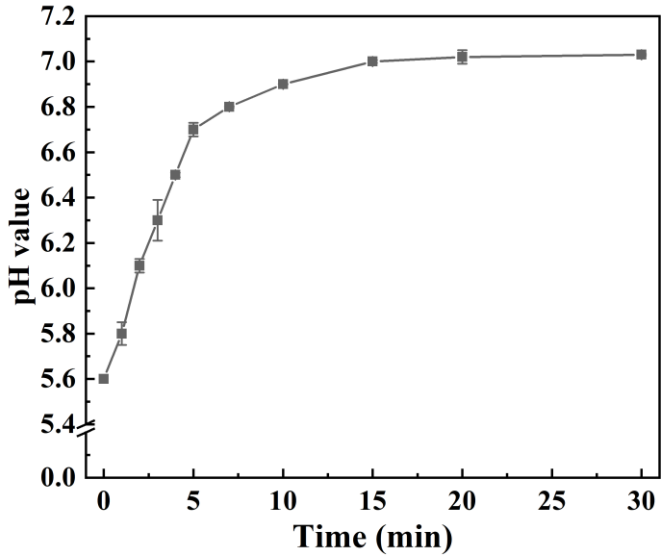

Figure S11. The variation of pH value with the reaction time during degradation process of PCMX by $Fe_{0.1}$-Mn-350. Conditions: $[PCMX]_0$ = 20 mg/L, [Cat.] = 0.2 g/L, pH_0 = 5.6.

.

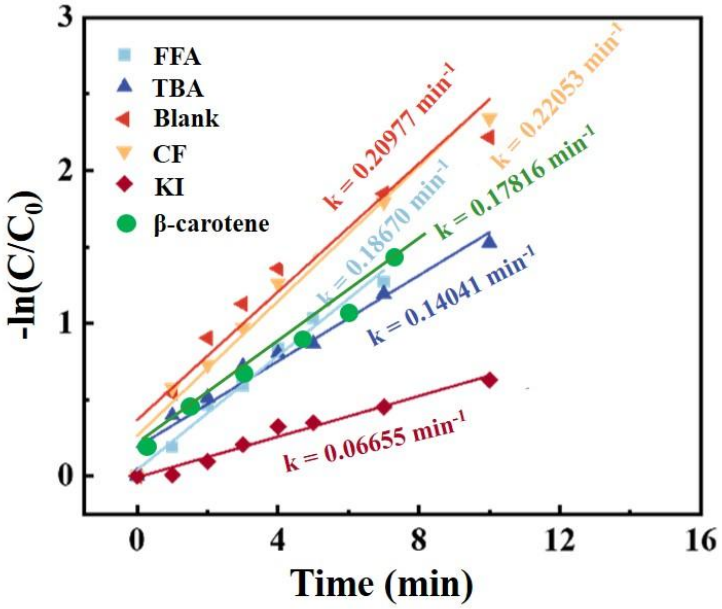

Figure S12. Degradation efficiency of PCMX with different quenchers in $Fe_{0.1}$-Mn-350/O_2 system.

Conditions: $[PCMX]_0$ = 20 mg/L, [Cat.] = 0.2 g/L, pH_0 = 5.6.

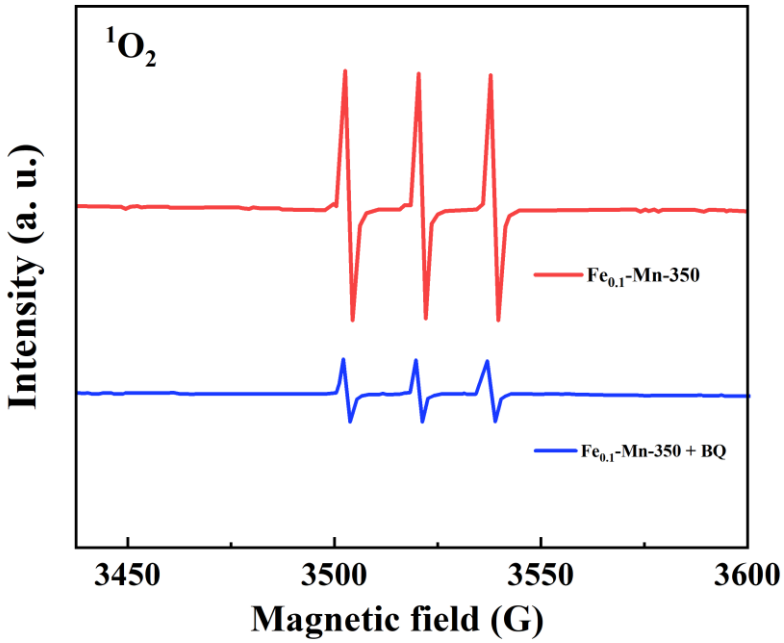

Figure S13. TEMP-based EPR spectra for the detection of $^1O_2$ in different systems. Conditions: [Cat.] = 0.2 g/L, [BQ] = 10 mM, pH_0 = 5.6, air atmosphere.

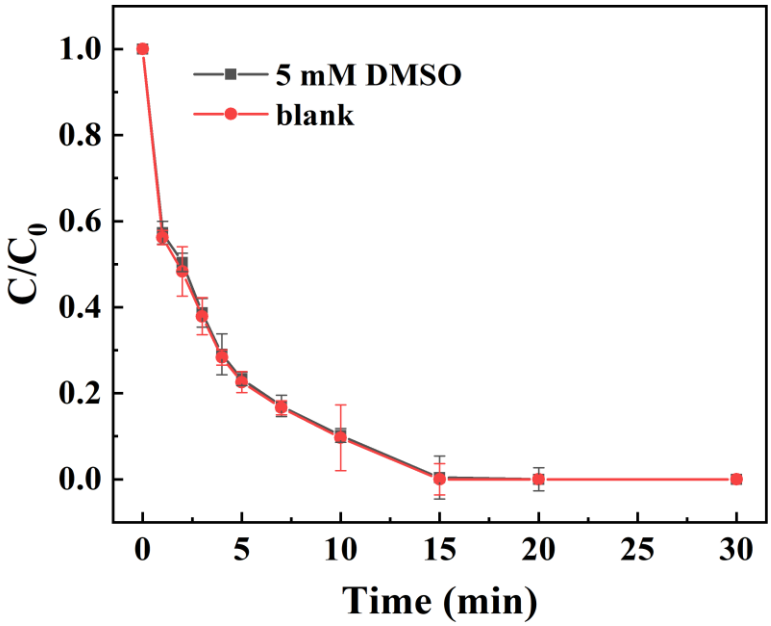

Figure S14. Effect of DMSO addition on degradation efficiency of PCMX in the $Fe_{0.1}$-Mn-350/N_2 system. Conditions: $[PCMX]_0$ = 20 mg/L, [Cat.] = 0.2 g/L, pH_0 = 5.6.

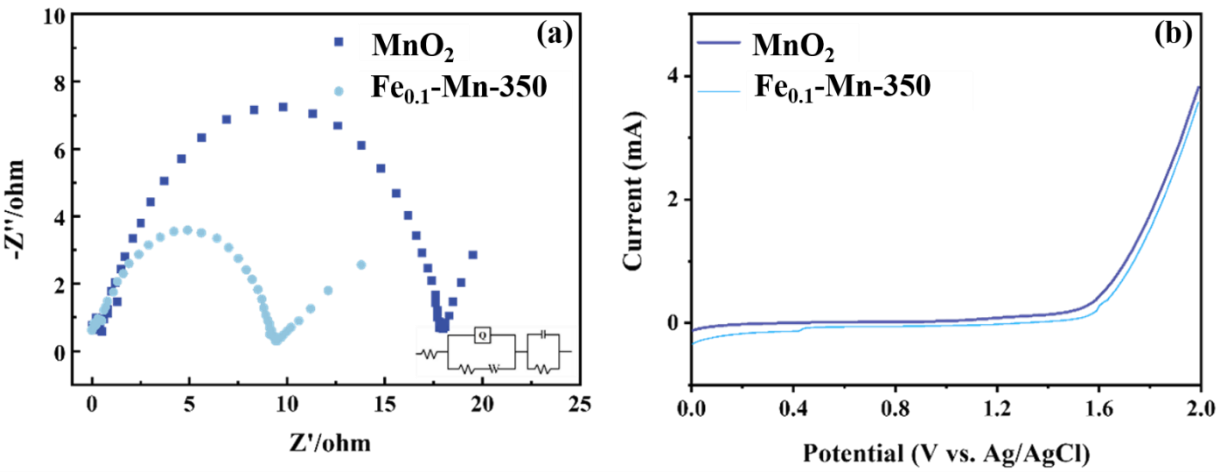

Figure S15. Electrochemical impedance spectroscopy analysis (a) and linear sweep voltammetry curve analysis (b) of $Fe_{0.1}$-Mn-350/O_2 system and MnO_2/O_2 system.

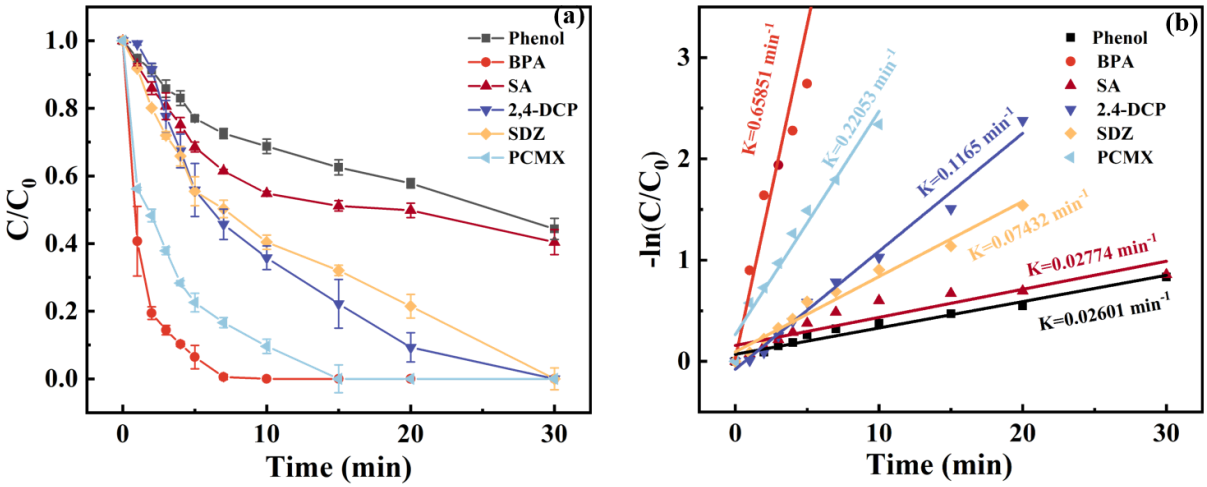

Figure S16. Degradation efficiency (a) and kinetics (b) of $Fe_{0.1}$-Mn-350/O_2 system for different ECs.

Conditions: $[ECs]_0$ = 20 mg/L, [Cat.] = 0.2 g/L, pH = 5.6.

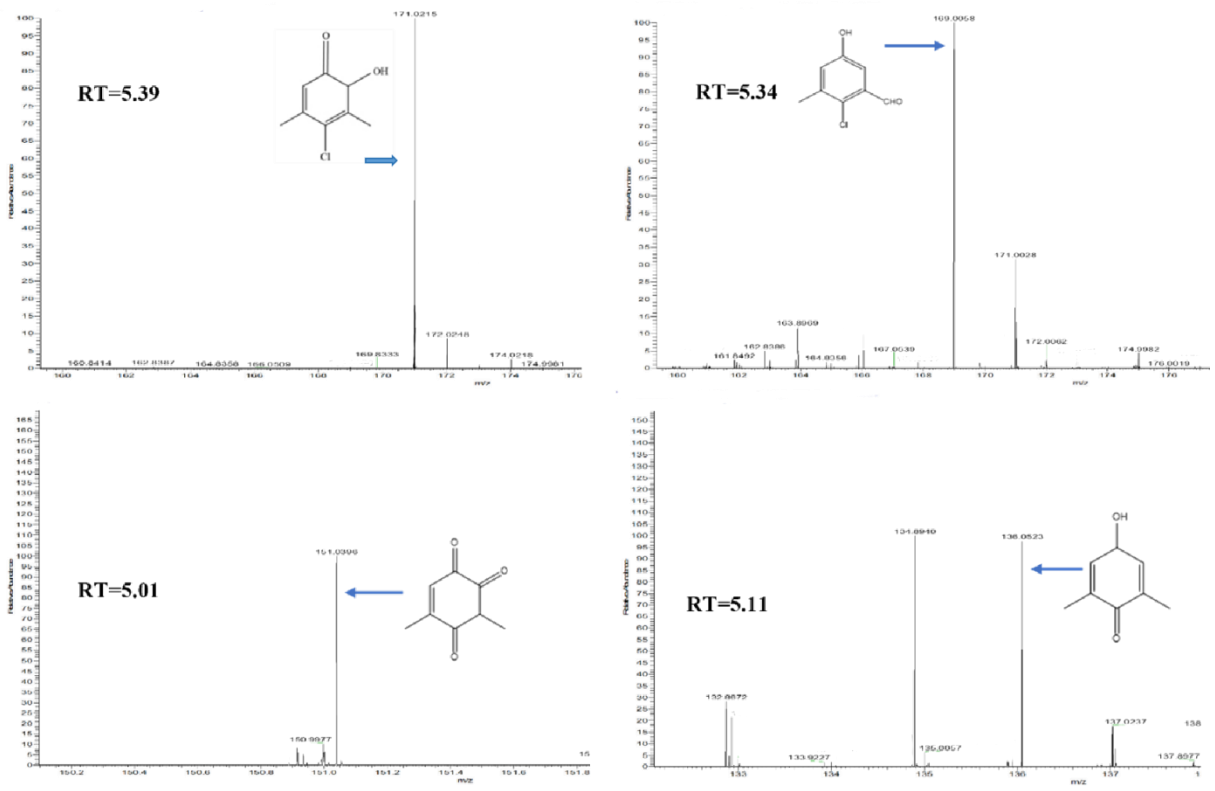

Figure S17. LC-MS particle flow diagram of PCMX degradation intermediates by the $Fe_{0.1}$-Mn-350/O_2 system.

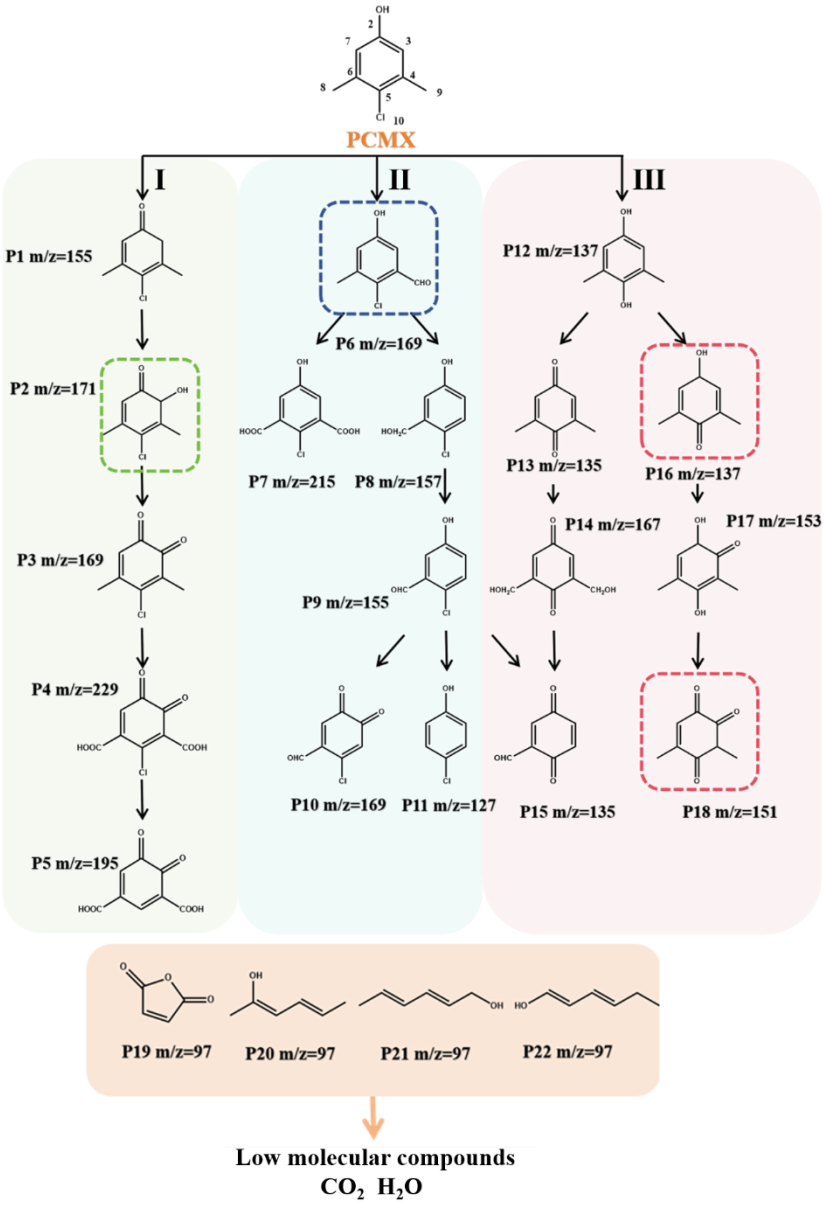

Figure S18. Proposed PCMX degradation pathways in $Fe_{0.1}$-Mn-350/O_2 system.

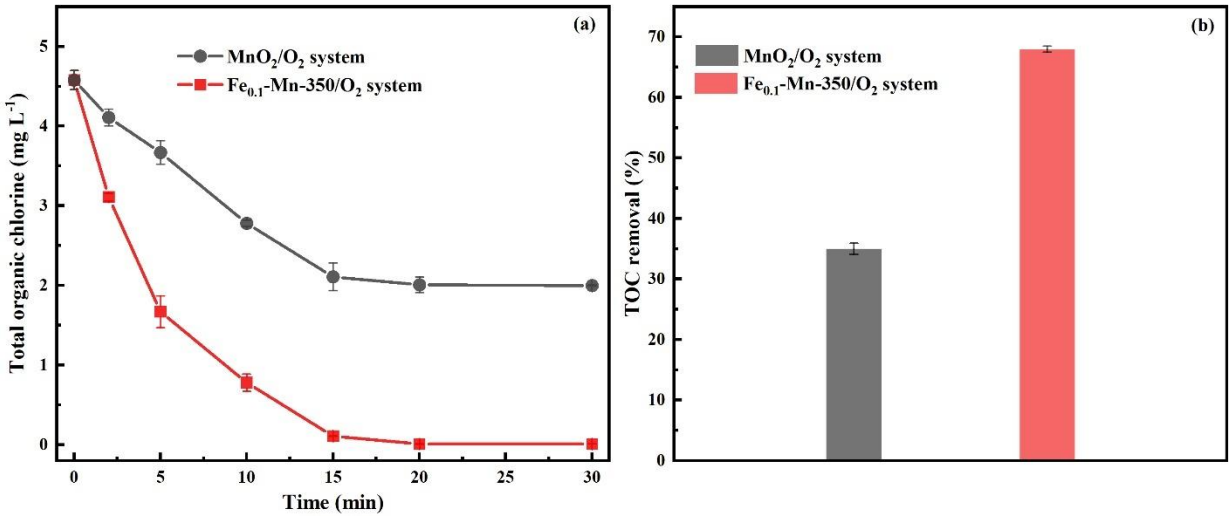

Figure S19. Concentration variation of total organic chlorine (TOC) in PCMX water sample treating with MnO_2/O_2 and $Fe_{0.1}$-Mn-350/O_2 systems. Conditions: $[PCMX]_0$ = 20 mg/L, [Cat.] = 0.2 g/L, pH_0 = 5.6.

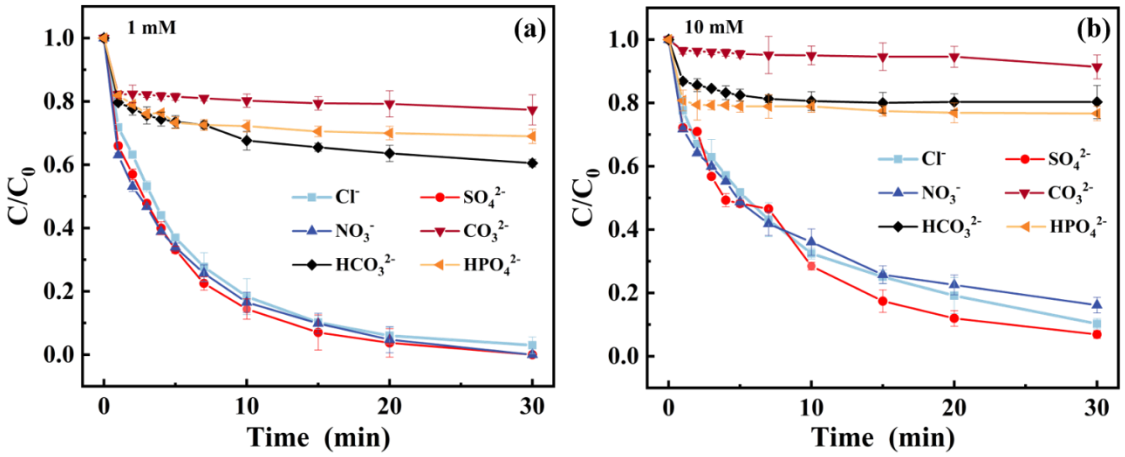

Figure S20. Effect of inorganic anions on the PCMX degradation in $Fe_{0.1}$-Mn-350/O_2 system. Conditions: $[PCMX]_0$ = 20 mg/L, [Cat.] = 0.2 g/L, pH_0 = 5.6.

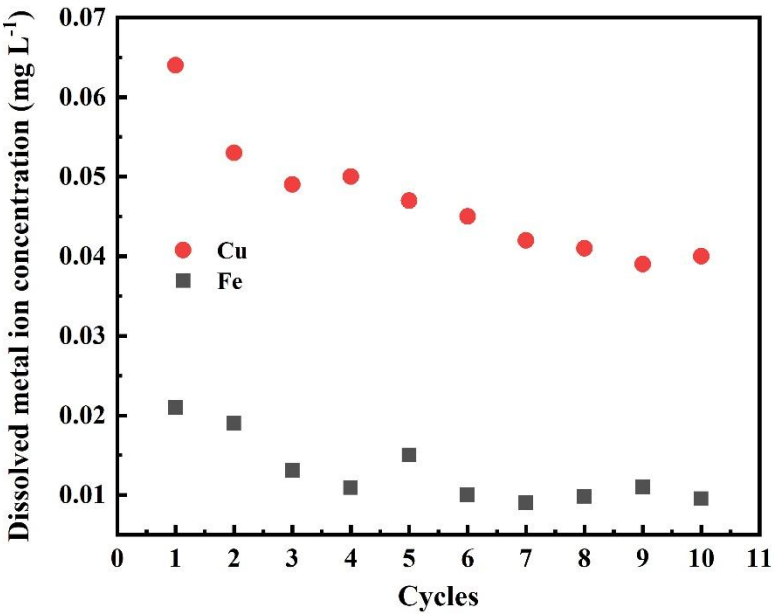

Figure S21. Cycling experiments on the concentration of Fe and Mn leaching. Conditions: $[PCMX]_0$ = 20 mg/L, [Cat.] = 0.2 g/L, pH_0 = 5.6.

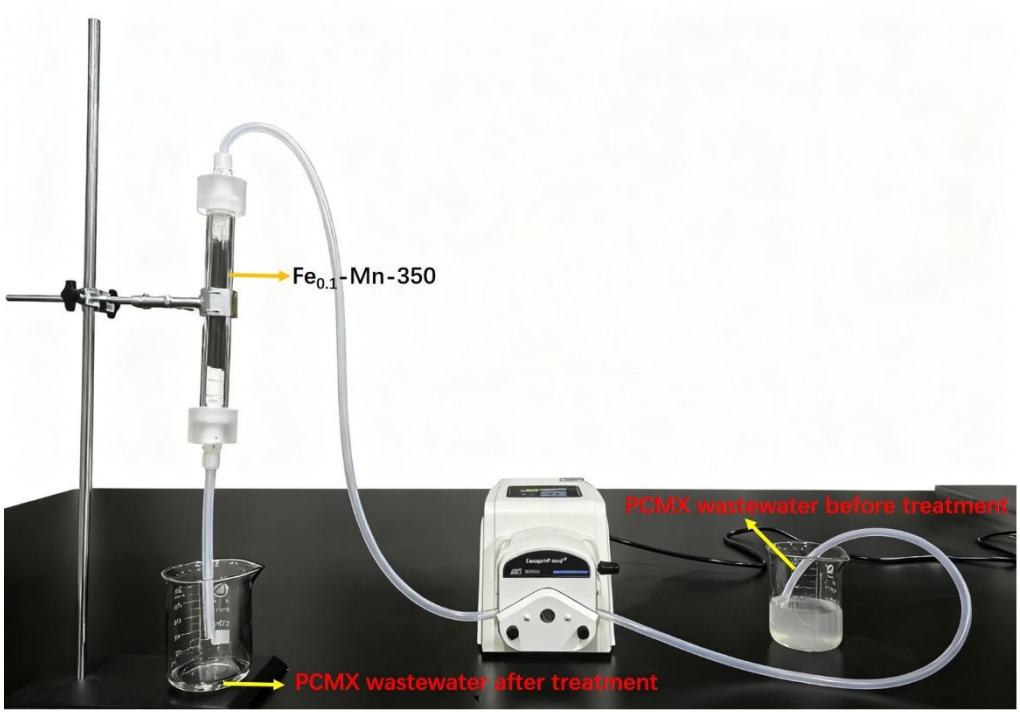

Figure S22. Schematic of a continuous flow column reactor unit for PCMX wastewater treatment.

Conditions: [Cat.] = 10 mg, $[PCMX]_0$ = 24 mg/L, water flow rate of 15 mL/h.

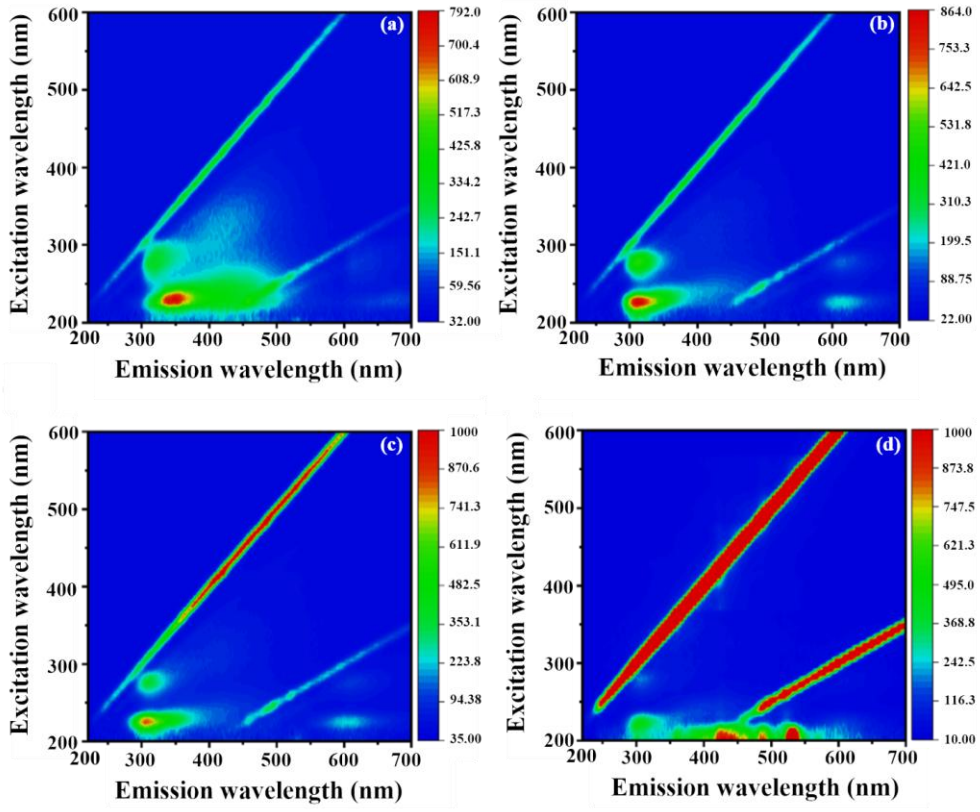

Figure S23. 3D fluorescence images of PCMX removal by the $Fe_{0.1}$-Mn-350/O_2 system in a river water matrix: river water matrix (a), river water containing 20 mg/L of PCMX (b), after 15 min (c) and 30 min (d) of treatment.

Table S1. Water quality parameters of real wastewater

Parameters	Values
Cl^- (mg/L)	237
CO_3^{2-} (mg/L)	0.64
HPO_4^{2-} (mg/L)	0.81
NO_3^- (mg/L)	17
SO_4^{2-} (mg/L)	55
NH_4^+-N (mg/L)	0.09
PCMX (mg/L)	24
COD (mg/L)	26
TOC (mg/L)	14
pH	6.1

The disinfected wastewater collected from a hospital in Ji'an city.

Table S2. Experimental details of HPLC

Organic	Mobile phase	Flow rate (mL/min)	Detection wavelength (nm)	Colum temperature (°C)
BPA	50% acetonitrile and 50% H_2O	0.4	227	36
PCMX	50% CH_3OH and 50% H_2O	1.2	223	40
phenol	50% acetonitrile and 50% H_2O	1	269	26
SDZ	20% acetonitrile and 80% H_2O	1	266	40
SA	50% acetonitrile and 50% H_2O	1	294	26

Table S3. Comparative performance of $Fe_{0.1}$-Mn-350 with representative catalysts for halogenated phenolic contaminant degradation.

Catalyst	Contaminant	Oxidant	k (min^{-1})	Time for complete degradation	Cycling performance	Synthesis/Cost note
$Fe_{0.1}$-Mn-350 (**This work**)	PCMX	O_2 (air)	0.2205	15 min (20 mg/L)	~75% (after 5 runs)	Hydrothermal-calcination, low-cost Fe/Mn
MIL-53(Fe)-NO_2 [5]	PCMX	H_2O_2	0.17	30 min	~98%	Ligand modification required
Fe SA/NPCs [6]	BPA	PMS	–	6 min	Significant drop	Readily available reagents
Fe SAC (for SMX) [7]	SMX	PMS	0.086	40 min	>90%	Cost ~1.63 USD/m^3
Periclase [8]	BPA	PMS	0.23	40 min	Excellent	Purification needed, higher cost
Co SAC [9]	BPA	PMS	0.0662	40 min	72.1% (acidic)	One-pot, noble metal precursor
Fe@Cu [10]	2,4-DCP	H_2O_2	0.1688	30 min	86.75%	Cu leaching risk
CuNi-NC [11]	4-CP	PMS	–	30 min	Stable in pH 3-11	Requires continuous PMS addition
Pd/Fe@PPY [12]	4-CP	Active H	–	60 min (50 mg/L)	–	Pd expensive, complex synthesis

Table S4. Contribution and generation of reactive species in $Fe_{0.1}$-Mn-350/O_2 system

Equation	Number	Reference
$fO_2^{\bullet-}, PCMX = \frac{K_{obs}-K_{CF}}{K_{obs}} \times 100\%$	(1)	[13, 14]
$f^{\bullet}OH\ (solution), PCMX = \frac{K_{obs}-K_{\mathrm{TBA}}}{K_{obs}} \times 100\%$	(2)	[13, 14]
$f^1O_2,\ PCMX = \frac{K_{obs}-K_{FFA}}{K_{obs}} \times 100\%$	(3)	[13, 14]
$f^{\bullet}OH\ (surface), PCMX = \frac{K_{obs}-K_{KI}}{K_{obs}} \times 100\%$	(4)	[13, 14]
$f\ Fe(IV), PCMX = \frac{K_{obs}-K_{DMSO}}{K_{obs}} \times 100\%$	(5)	[13, 14]
$e^- + O_2 \rightarrow O_2^{\bullet-}$	(6)	[15-17]
$2O_2^{\bullet-} + H_2O \rightarrow H_2O_2 + {}^1O_2 + OH^-$	(7)	[15-17]
$H^+ + O_2^{\bullet-} \rightarrow HO_2^{\bullet}$	(8)	[15-17]
$2HO_2^{\bullet} \rightarrow H_2O_2 + {}^1O_2$	(9)	[15-17]
$HO_2^{\bullet} + O_2^{\bullet-} \rightarrow HO_2^- + {}^1O_2$	(10)	[15-17]

Table S5. Adsorption energies of O_2 in end-on and side-on forms adsorbed between bi-Fe sites

Combination method	E_{total} (a)	$E_{substrate}$ (Ha)	E_{O_2} (Ha)	E_{ads} (eV)
end-on	-327.61658	-9.92	-315.41848	-2.2781
side-on	-328.26973	-9.92	-315.41848	-2.93125

E_{total}: The total energy of the ideal adsorption structure.

$E_{substrate}$: The total energy of $Fe_{0.1}$-Mn-350.

E_{ads}: The adsorption energy of O_2 on $Fe_{0.1}$-Mn-350. A negative value of Eads indicates exothermic adsorption, and the larger the absolute value, the more favorable the adsorption process.

Table S6. Iron leaching and loss rate per cycle

Cycle	Fe leaching (mg/L)	Fe leached per batch (μg)	Fe loss rate (%)
1	0.0215	1.075	10.75
2	0.0185	0.925	9.25
3	0.0135	0.675	6.75
4	0.0115	0.575	5.75
5	0.0150	0.750	7.50
6	0.0100	0.500	5.00
7	0.0090	0.450	4.50
8	0.0098	0.490	4.90
9	0.0110	0.550	5.50
10	0.0095	0.475	4.75

Table S7. Economic comparison of different treatment technologies

Cost item	$Fe_{0.1}$-Mn-350 system	PMS-activation process	Fenton treatment
Reference	this study	[18-21]	[22-24]
Catalyst cost	0.25 US$/m^3	0.50-0.85 US$/m^3	0.35 US$/m^3
Oxidant cost	0 (air)	0.80 US$/m^3 (PMS)	0.30 US$/m^3 ($H_2O_2$)
pH adjustment	0	0	0.15 US$/m^3
Sludge handling	0	0	0-0.25 US$/m^3
Energy consumption	0.03 US$/m^3 (500 rpm)	0.15-0.35 US$/m^3 (UV/electric field)	0.05-0.10 US$/m^3 (UV/ultrasound/ electric field)
Total treatment cost	0.28 US$/m^3	1.45-2.00 US$/m^3	0.85-1.15 US$/m^3

Reference

[1] W. Zheng, L. Zhu, S. Liang, J. Ye, X. Yang, Z. Lei, Z. Yan, Y. Li, C. Wei, C. Feng, Discovering the Importance of ClO• in a Coupled Electrochemical System for the Simultaneous Removal of Carbon and Nitrogen from Secondary Coking Wastewater Effluent, Environmental Science & Technology, 54 (2020) 9015-9024.

[2] S. Lungu-Mitea, C. Vogs, G. Carlsson, M. Montag, K. Frieberg, A. Oskarsson, J. Lundqvist, Modeling Bioavailable Concentrations in Zebrafish Cell Lines and Embryos Increases the Correlation of Toxicity Potencies across Test Systems, Environmental Science & Technology, 55 (2021) 447-457.

[3] H. Gu, X. Liu, X. Liu, C. Ling, K. Wei, G. Zhan, Y. Guo, L. Zhang, Adjacent single-atom irons boosting molecular oxygen activation on MnO2, Nature Communications, 12 (2021) 5422.

[4] D. Yang, Y. Guo, Z. Yu, Z. Jiang, W. Xiang, X. Wu, J. Wang, Surface Oxygen Vacancy Engineering for Enhanced Volatile Organic Compounds Removal in Solar-Interfacial Water Evaporation, Environmental Science & Technology, 59 (2025) 7117-7128.

[5] J. Sun, S. Li, H. Wang, L. Zhu, Y. Chen, J. Zhu, H. Ma, X. Xiao, T. Liu, Nitro-functionalization on MIL-53(Fe) for PCMX degradation: Elevating Fenton-like catalytic propelled by abundant reaction sites and iron cycle, Chemosphere, 362 (2024) 142707.

[6] L. Yang, H. Yang, S. Yin, X. Wang, M. Xu, G. Lu, Z. Liu, H. Sun, Fe Single-Atom Catalyst for Efficient and Rapid Fenton-Like Degradation of Organics and Disinfection against Bacteria, Small, 18 (2022) 2104941.

[7] C. Wang, H. Liu, P. Sun, J. Cai, M. Sun, H. Xie, G. Shen, A novel peroxymonosulfate activation process by single-atom iron catalyst from waste biomass for efficient singlet oxygen-mediated degradation of organic pollutants, Journal of Hazardous Materials, 453 (2023) 131333.

[8] L. Kong, G. Fang, X. Xi, Y. Wen, Y. Chen, M. Xie, F. Zhu, D. Zhou, J. Zhan, A novel peroxymonosulfate activation process by periclase for efficient singlet oxygen-mediated degradation of organic pollutants, Chemical Engineering Journal, 403 (2021) 126445.

[9] Q. Wang, C. Liu, D. Zhou, X. Chen, M. Zhang, K. Lin, Degradation of bisphenol a using peroxymonosulfate activated by single-atomic cobalt catalysts: Different reactive species at acidic and alkaline pH, Chemical Engineering Journal, 439 (2022) 135002.

[10] S. Yang, Y. Huang, Y. Du, J. Wang, B. Liu, G. Han, Efficient degradation of chlorinated phenolic compounds by Fe@Cu materials with enhanced oxygen reduction reaction, Separation and Purification Technology, 318 (2023) 124047.

[11] X. Zhang, K. Tian, J. Mao, X. Liu, T. Qing, Pomelo peel biochar loaded Cu-Ni bimetallic catalysts with low metal leaching for efficient peroxymonosulfate activation and 4-chlorophenol removal, Journal of Environmental Chemical Engineering, 13 (2025) 119137.

[12] C. Lei, Z. Zhou, W. Chen, J. Xie, B. Huang, Polypyrrole supported Pd/Fe bimetallic nanoparticles with enhanced catalytic activity for simultaneous removal of 4-chlorophenol and Cr(VI), Science of The Total Environment, 831 (2022) 154754.

[13] H. Zhu, A. Guo, S. Wang, Y. Long, G. Fan, X. Yu, Efficient tetracycline degradation via peroxymonosulfate activation by magnetic Co/N co-doped biochar: Emphasizing the important role of biochar graphitization, Chemical Engineering Journal, 450 (2022) 138428.

[14] H. Xiao, Y. Wang, K. Lv, C. Zhu, X. Guan, B. Xie, X. Zou, X. Luo, Y. Zhou, N-doped biochar-Fe/Mn as a superior peroxymonosulfate activator for enhanced bisphenol a degradation, Water Research, 278 (2025) 123399.

[15] H. Xiao, B. Jiang, Z. Zhang, C. Zhu, J. Chen, Y. Wang, Y. Dong, Y. Hao, Y. Liu, Y. Li, X. Xiao, G. He, Y. Zhou, X. Luo, New insight of electrogenerated H_2O_2 into oxychlorides inhibition and decontamination promotion: from radical to nonradical pathway during anodic oxidation of high Cl^--laden wastewater process, Journal of Hazardous Materials, (2024) 136948.

[16] H. Kang, Y. Chen, M. Cheng, H. Guo, W. Ren, G. Zhang, W. Zhou, Q. Shi, C. Zhao, B. Zou, Q. Wang, Z. Yuan, Optimization of electronic structure by constructing bimetallic system for refractory wastewater purification: Tailoring the efficient selective generation of singlet oxygen, Chemical Engineering Journal, 522 (2025) 167255.

[17] S. Jo, H. Kim, K. Eun Lee, S. Hong, K. Cho, S. Kim, G.-h. Moon, J. Lim, Unraveling Janus-like behavior of copper phosphide for selective production of reactive oxygen species: Singlet oxygen versus hydroxyl radical, Chemical Engineering Journal, 470 (2023) 144389.

[18] Q. Fang, H. Yang, S. Ye, P. Zhang, M. Dai, X. Hu, Y. Gu, X. Tan, Generation and identification of 1O2 in catalysts/peroxymonosulfate systems for water purification, Water Research, 245 (2023) 120614.

[19] J. Yang, M. Zhu, D.D. Dionysiou, What is the role of light in persulfate-based advanced oxidation for water treatment?, Water Research, 189 (2021) 116627.

[20] S. Liu, Z. Zhang, F. Huang, Y. Liu, L. Feng, J. Jiang, L. Zhang, F. Qi, C. Liu, Carbonized polyaniline activated peroxymonosulfate (PMS) for phenol degradation: Role of PMS adsorption and singlet oxygen generation, Applied Catalysis B: Environmental, 286 (2021) 119921.

[21] Y. Du, J.-Y. Cao, Y. Lu, H. Zhang, J. Zhang, Y. Shi, B. Lai, Cytotoxicity and Genotoxicity toward Mammalian Cells Induced by Organic Iodine in Peroxymonosulfate (PMS) Processes: Activated PMS Is Better than Nonactivated PMS in Mitigating Toxicity, Environmental Science & Technology, 59 (2025) 5925-5935.

[22] C. Yang, S. Shang, L. Lin, P. Wang, Z. Ye, Y. Wang, K. Shih, L. Sun, X.-y. Li, Electro-driven cycling Fenton catalysis through two-dimensional electroresponsive metal–organic frameworks for water purification, Nature Water, 2 (2024) 793-802.

[23] J. Zheng, H.J. Lim, T. Hedtke, J.-H. Kim, S. Zhang, Manganese oxide for heterogeneous Fenton treatment: Catalyst or inhibitor?, Applied Catalysis B: Environment and Energy, 359 (2024) 124531.

[24] Z.-S. Zhu, Y. Wang, P. Wang, S. Zhong, K. Hu, S. Ren, J.P. Vongsvivut, H. Sun, X. Duan, S. Wang, Multidimensional engineering of single-atom cobalt catalysts for ultrafast Fenton-like reactions, Nature Water, 3 (2025) 211-221.